THE JOURNAL OF PHYSICAL CHEMISTRY B

Article

pubs.acs.org/JPCB

Effects of Spacer Length and Terminal Group on the Crystallization and Morphology of Biscarbamates: A Longer Spacer Does Not Reduce the Melting Temperature

Mostofa Kamal Khan and Pudupadi R. Sundararajan*

Department of Chemistry, Carleton University, 1125 Colonel By Drive, Ottawa, Ontario K1S 5B6, Canada

Supporting Information

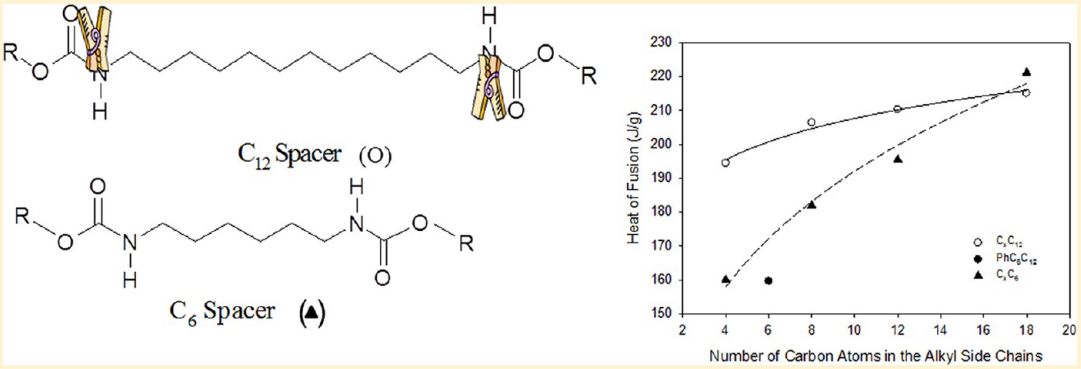

ABSTRACT: The effects of alkyl side chain and spacer lengths and the type of terminal group on the morphology and crystallization of a homologous series of biscarbamates (model compounds for polyurethanes) were investigated. Biscarbamates were synthesized with alkyl side chains of various lengths ranging from C_4 to C_{18} and an alkyl spacer group with 12 CH_2 units (C_{12} spacer) between the two hydrogen bonding motifs. The crystallization and morphological features are compared with the previously studied biscarbamates with a C_6 spacer. As a token example, we also studied a biscarbamate molecule in which the terminal methyl group was replaced by a phenyl group. We stress four important conclusions of the study: (1) A number of studies in the literature found that the longer alkyl spacers reduced the thermal transition temperatures of the molecules, and such behavior was attributed to an increase in the flexibility of the alkyl spacer. However, the results of the present study are to the contrary. With the biscarbamates studied here, the hydrogen-bonding groups on both sides of the C_{12} spacer act as "anchors", and the longer spacer does not reduce the melting temperatures compared with those with the C_6 spacer. (2) The melt viscosity measurements show shear-thinning behavior, which has been mostly observed with polysaccharides and hydrogen-bonded polymers. (3) Avrami analysis shows a two-stage crystallization, which is not commonly observed in organic small molecule systems. (4) The phenyl end group does not add another self-assembly code in terms of π-stacking but acts as a defect. While formation of crystals was observed for biscarbamates with short alkyl side chains with a C_6 spacer, an increase in spacer length to C_{12} induces spherulitic morphology. Although the overall sizes of the spherulites are the same for both spacers, the rate of spherulite growth was higher and the crystallization rate was lower with the C_{12} spacer compared with the C_6 spacer. In contrast with the biscarbamates containing C_6 spacer previously studied, we find that among the biscarbamates with 12 CH_2 units in the spacer the C_{12}−C_{12} molecule shows the minimum spherulite size, spherulite growth rate, and rate of crystallization. The infrared frequency shifts of the N−H group due to hydrogen bonding were used to calculate the N···O hydrogen-bonding distance and found to be close to the value observed in the crystal structure of the biscarbamate with a C_6 spacer and C_{10} alkyl side chain.

INTRODUCTION

A significant research effort has so far been invested in the understanding of molecular self-assembly mediated by noncovalent interactions. Although these interactions themselves are rather weak, collectively, they result in the formation of very stable molecular aggregates. Among the various noncovalent interactions leading to molecular self-assembly, hydrogen-bond-mediated self-assembly has been extensively studied in recent years to create supramolecular architectures of specific dimensions and functionality.[1,2] It was seen that extended supramolecular assembly requires selectivity, self-complementarity, and orthogonality of recognition events that can be achieved by the incorporation of multiple hydrogen-bond donor−acceptor moieties in the molecules. Hydrogen bonding has thus been utilized in the design of oligomers with specific secondary structures,[3] molecular strands employed in specific modes of intermolecular aggregates,[4] self-organization of

Received: October 2, 2012
Revised: April 13, 2013
Published: April 15, 2013

Scheme 1

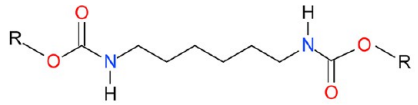

C_6 Spacer

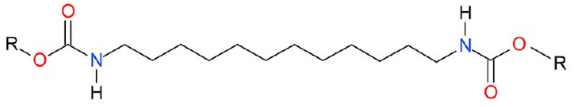

C_{12} Spacer

R : n-alkyl chain with number of C atoms ranging from 4 to 18

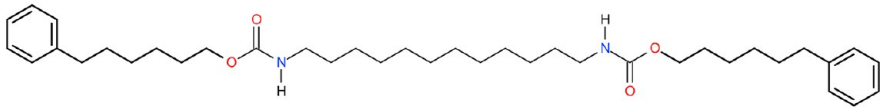

C_{12} Spacer; phenyl end groups

dendritic macromolecules,[5] and polymers with noncovalent main chains and side chains.[6]

Whereas the appropriate design of molecules with hydrogen bonding moieties leads to supramolecular assembly, controlling the morphology of the structures created by such assembly still remains a challenge. Moreover, depending on the conditions of solidification, molecular self-assembly may lead to the formation of single crystals, spherulites, or gels of the materials. If a process, for example, allows the material to solidify with large spherulitic morphology, the resultant solid would suffer from brittleness and the lack of optical clarity. It thus becomes essential to tailor both the molecular structure and the process protocol to achieve the desired morphology and functionality of the materials. To this end, we have been studying the influence of side-chain length as well as single versus double hydrogen-bond motifs on the morphology and miscibility behavior upon crystallization, blending, and gelation of a class of hydrogen-bond-mediated self-assembling system of carbamates[7] and biscarbamates.[8] The effect of carbon atom parity on the crystallization and morphology has also been studied.[9] It was shown that although hydrogen bond mediates the self-assembly in these cases, the van der Waals interactions arising from the alkyl side chains have a profound influence on the crystallization and morphology.

Carbamates and biscarbamates have long been studied for their importance in scientific and technological applications. Scientific studies of these classes of molecules date back to the early 1900s. Gaylord[10] investigated acetylene biscarbamates in the early 1950s. The hydrogen-bond-mediated self-assembly of these molecules mimics that of biological systems. Furer[11] investigated infrared spectra of carbamates to probe into the hydrogen-bonding characteristics of the molecules. The potential applications are diverse, ranging from organic intermediates to serving as model compounds for studying polyurethane properties.[12−24] Carbamates with alkyl side chains have a melt viscosity of about 8−12 cP and melting temperatures of 60−90 °C and crystallize rapidly upon quenching from the melt. These suitable properties made them potential candidates as ink vehicles for inkjet printing technologies.[25−27]

Our previous studies[7−9] were concerned with the crystallization behavior and morphology of *N*-octadecyl carbamates (referred therein as simple or monocarbamates) and biscarbamates with alkyl side chains of various lengths ranging from C_4 to C_{18}. The former contains one hydrogen-bonding motif and asymmetric side chains on either side (except C_{18}), while the biscarbamates have two hydrogen-bonding sites flanked by symmetric side chains in length. The two hydrogen bonding groups are separated by a C_6 spacer. These differences in the molecular architecture led to differences in crystallization and morphology. The monocarbamates showed an increase in spherulite size with the alkyl side chain length. However, with biscarbamates, the maximum spherulite size and growth rate were observed for a C_8 alkyl side chain. Relative contributions of hydrogen-bond and van der Waals forces dictate such behavior. In another work,[28] we showed that blends of any two biscarbamates self-sort and show immiscibility and molecular selectivity and the alkyl side chains play a role in such selectivity and immiscibility.

In this work, we discuss the influence of spacer group length and the type of terminal group (i.e., methyl vs phenyl) of the alkyl side chains on the morphology and thermal behavior of a set of biscarbamates. We synthesized a series of molecules containing a spacer group that is twice the length of that of the previously studied biscarbamates and with alkyl side chains of variable length symmetrically attached to the hydrogen-bonding moieties. For the purpose of this study, we designate these molecules as C_x−C_6 and C_x−C_{12}, where x refers to the number of carbon atoms in the alkyl side chains and numbers 6 or 12 refer to the number of CH_2 units in the spacer group between the hydrogen-bonding moieties. We also synthesized a token compound with alkyl side chains terminated with phenyl groups and designate it as PhC_6−C_{12}. The molecules studied here are shown in Scheme 1.

Whereas a number of studies[29−33] in the literature observed a decrease in melting and other thermal transition temperatures with an increase in alkyl spacer length, our results are to the

dx.doi.org/10.1021/jp309762a | J. Phys. Chem. B 2013, 117, 5705−5717

contrary in the present study, as discussed later. We believe that in the present case, the increase in spacer length would lead to an increase in the relative contribution of the van der Waals forces with respect to that of hydrogen bonding, which remains constant in all of the molecules in this series. This, in turn, would result in thermal and crystallization properties different from those observed with a $(CH_2)_6$ spacer. The substitution of the terminal methyl group with a bulky phenyl group is expected to affect the molecular organization of the molecules. Because thermal properties, rates of spherulite growth, and crystallization are important attributes in applications such as inkjet ink vehicles, in this study, we discuss the above properties of these molecules and compare them with previously studied biscarbamates with different spacer length and alkyl-terminal groups.

EXPERIMENTAL SECTION

Biscarbamates with different lengths of spacer group and alkyl side chains were synthesized as described in our previous publications[8a,34] from the appropriate diisocyanates and alcohols.

A TA Instruments 2010 differential scanning calorimeter was used for thermal analysis at a heating rate of 10 °C/min. The calorimeter was calibrated for temperature and energy with an indium sample as a standard reference material. DSC traces were recorded in a nitrogen atmosphere with 7−10 mg of the sample taken in an aluminum pan. For studies on isothermal crystallization kinetics, the samples were heated to a temperature of ∼40 °C above their melting points (T_m) and then allowed to cool to a temperature 5 °C above their crystallization temperatures. The samples were then cooled to their crystallization temperature at a rate of 1 °C/min and allowed to stay at isothermal condition for 30 min. The heat of crystallization was measured at 0.6 s intervals, and the crystallinity was determined by integrating the isothermal heat flow curve with respect to time. The fractional degree of crystallization (α) was calculated by the ratio of the heat of crystallization at time t to the total heat of crystallization using the following equation.

$$\alpha = \frac{\Delta H_t}{\Delta H_\infty} = \frac{\int_0^t \frac{dQ}{dt}\, dt}{\int_0^\infty \frac{dQ}{dt}\, dt} \quad (1)$$

where ΔH_t is the partial area between the DSC curve and the time axis at time t and ΔH_∞ is the total area under the peak that corresponds to the total heat of crystallization. The $t_{1/2}$ of a sample was calculated by plotting the fractional degree of crystallization (α) with respect to time (t). All DSC thermograms were recorded using Thermal Advantage software, and the data were processed by TA Universal Analysis software.

The isothermal crystallization data were plotted in the form of the Avrami equation

$$\ln(-\ln[1 - X(t)]) = \ln K + n \ln t \quad (2)$$

where $X(t)$ is the crystalline fraction at time t and K and n are the Avrami parameters.

Optical micrographs were recorded on a Zeiss Axioplan polarized optical microscope (POM). Northern Eclipse (version 8.0) image-processing software was used to capture the images as well as to calculate the spherulite size. Samples for optical microscopy were prepared by melting a small amount of the material on a microscope slide with a cover slide at a temperature of T_m + 20 °C, holding it isothermally for 10 min to remove morphological history if there was any, and then cooling it slowly to room temperature at the rate of ∼5 °C/min. These are referred to as slow-cooled (SC) samples. Another set of samples was prepared following the same procedure but by quenching the samples (Q-samples) immediately to room temperature from the melt. For the kinetic study of the spherulite growth, a Linkam LTS 350 hot stage equipped with a Linkam TMS 94 thermocontroller was used. For these studies, the samples were placed on a microscope slide with a cover glass (as mentioned above), were heated to a temperature 20 °C above that of the melting temperature of the biscarbamate at a rate of 5 °C/min, and were held at that temperature for ∼10 min. They were then cooled at a rate of 2 °C/min to a temperature of 5 °C above the crystallization temperature (T_c) and then at the rate of 0.1 °C/min to the T_c. The Northern Eclipse image processing software was used to capture the images at specific time intervals during the crystallization and calculate the spherulite size by subsequent data processing. Because microscope slides with cover were used for the preparation of SC and quenched samples as well as for the hot stage microscopy, no difference in the spherulitic morphology is expected due to the positioning of the sample.

Melt viscosities were measured using an Anton Paar MCR502 rheometer. This rheometer offers minimum torque of 10 nN·m and torque resolution of 0.1 nM·m, which enables one to measure the rheological properties of very low viscosity materials. All of the measurements were performed at a temperature of 130 °C with a cone-and-plate geometry with an angle of 1° and diameter of 25 mm.

The experimental procedures that we followed for X-ray diffraction and IR spectroscopy have been given in detail in our previous publications[9] and are not included here.

RESULTS AND DISCUSSION

The purpose of this study is to determine the effects of the longer spacer and the phenyl end group on the thermal properties and rates of spherulite growth and crystallization in comparison with the C_6 spacer and methyl end groups.

Thermal Behavior. The biscarbamates studied here showed a single sharp transition in the DSC corresponding to their melting in the heating cycle and crystallization from melt to solid in the cooling cycle, as shown in Figure S1 (Supporting Information). The melting temperatures of these compounds are given in Table S1 in the Supporting Information and Figure 1 along with those of the homologous biscarbamates with a $(CH_2)_6$ spacer between the hydrogen-bonding moieties. These values are within ±0.4 °C based on at least three different measurements. It is seen from Figure 1a and Table S1 in the Supporting Information that the T_m of C_4−C_{12} is 10 °C higher than that of C_4−C_6. The difference decreases with the alkyl side-chain length. The T_m of C_{18}−C_{12} is lower than C_{18}−C_6 by only 3 °C. On the basis of the work of several authors,[29−33] one would expect that an increase in spacer length would lead to an increase in molecular flexibility and decrease the melting temperature. We see a significant departure in this work. In what follows, we offer an explanation of this behavior, contrasting with those in the literature.

It has been shown in the case of polyurethanes,[29] polyamides,[30] polyimides,[31,32] and liquid-crystalline polymers[33] that increasing the alkyl spacer length in the main chain

dx.doi.org/10.1021/jp309762a | J. Phys. Chem. B 2013, 117, 5705−5717

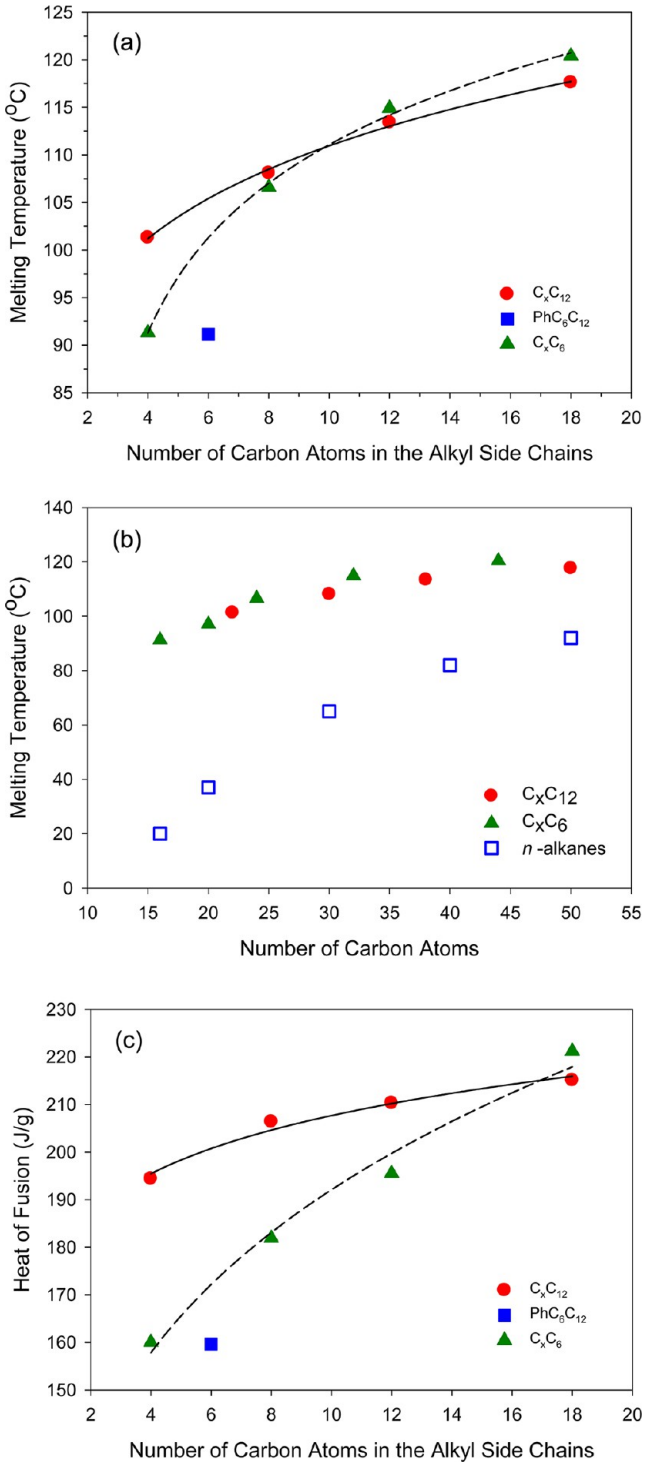

Figure 1. Variation of (a) melting temperature of biscarbamates as a function of alkyl side-chain length with $(CH_2)_6$ (----) and $(CH_2)_{12}$ (——) spacers, (b) T_m as a function of the total number of carbon atoms in the biscarbamates and *n*-alkanes, and (c) heats of fusion. The T_m and H_f for the phenyl-terminated C_6–C_{12} are also shown in panels a and c.

decreases the transition temperatures. This has been attributed to an increase in the flexibility of the spacer. It may be argued that an increase in alkyl spacer length would increase the T_m. Ethane has a T_m of −183 °C, hexadecane $[CH_3\text{-}(CH_2)_{14}\text{-}CH_3]$ melts at just about room temperature (20 °C), triacontane $[CH_3\text{-}(CH_2)_{28}\text{-}CH_3]$ melts at 65 °C, and polyethylene melts at 135 °C. Only two skeletal conformations, tt and tg (gt), are preferred for linear alkyl chains including polyethylene. The gg conformation is relegated to the segments in the chain fold. The difference between the tt and tg conformations is only 500 cal·mol^{-1}. Such a small difference in conformational energy should, in fact, lead to a highly flexible coil. However, the rather high T_m of polyethylene is due to the intermolecular packing of the chain segments and the van der Waals interaction between the trans–trans sequences. In the cases mentioned above,[29−33] the alkyl chain is flanked by other groups, and this leads to a different behavior. It is known that any branching in polyethylene would disrupt the interaction between the all-trans segments and reduce the T_m to as low as 95 °C.

With aliphatic (*m*,*n*) polyurethanes of the type $\text{-}[\text{O-}(CH_2)_m\text{-O-C(O)-NH-}(CH_2)_n\text{-NH-C(O)}]_x\text{-}$, McKiernan et al.[29b] found that increasing *m* (with *n* constant) or *n* (with *m* constant) led to a decrease in T_m. For example, with (*m*,*n*) = (2,6), (10,6), (22,6), and (32,6), the T_m values were 166, 161, 146, and 143 °C, respectively. Likewise, with (*m*,*n*) = (32,4), (32,6), (32,8), and (32,12), the T_m values were 150, 143, 139, 135 °C, respectively. Ehrenstein et al.[30] described the synthesis and properties of polyamide (6,24) and (6,34), containing long aliphatic segments (Scheme 2).

Scheme 2. Polyamide (6,*x*) with *x* = 22 or 32 (ref 30)

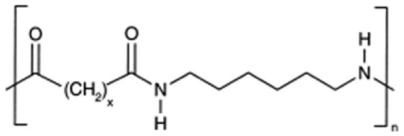

Whereas the T_m for polyamide (6,6) is 264 °C, it decreased to 189 and 177 °C, respectively, for polyamide (6,24) and (6,34). Although N–H···C=O hydrogen bonds are present in these polymers similar to the biscarbamates discussed here, the disposition of the hydrogen-bonding groups relative to the alkyl segment is different (compare Schemes 1 and 2). In the case of a polyimide, Yin et al.[31] found the T_m of α,ω-(di(4-aminophenoxy)) alkanes (monomer segment for the polyimides) to decrease with an increase in the length of the alkane segment. For C_2, C_4, C_6, C_8, C_{10}, and C_{12}, the T_m values were found to be 178, 136, 117, 116, 115, and 97 °C, respectively. For the corresponding polyimides, the glass-transition temperatures (T_g) were 237.3, 218.3, 186.9, 155.7, 153.7, and 142.6 °C, respectively, decreasing almost linearly with alkane segment length. The decrease in the T_m of the monomer segment and the T_g of these polyimides was attributed to the increased flexibility with the length of the alkane segment. In this case, only aromatic interactions occur and not hydrogen bonding. In another study of polyimides incorporating α,ω-(diamino) alkanes, Koning et al.[32] found that increasing the length of the alkane spacer from C_2 to C_9 in the polyimide (based on 3,3′,4,4′-benzophenonetetracarboxylic dianhydride) decreased the T_m from 400 to 138 °C (table 1 of ref 32). The T_g decreased as well from about 220 to 120 °C. In a review on liquid crystalline polymers, Ober et al.[33] noted that for *p*-phenylene-based polymers both the melting and the transition temperatures decreased with an increase in alkyl spacer length. For example, the melting temperature decreased from 340 °C for the C_2 spacer to 175 and 220 °C for the C_9 and C_{12} spacers, respectively.

dx.doi.org/10.1021/jp309762a | J. Phys. Chem. B 2013, 117, 5705−5717

In all of the examples cited above, an increase in the length of the alkyl spacer reduces the melting temperature of the polymer. Whereas this has been considered to be due to the enhanced flexibility of the alkyl spacer, this could be simply due to the disruption of the efficient packing of the alkyl chain by the groups attached to its either side and vice versa. For example, with the α,ω(-di(4-aminophenoxy) alkanes used by Yin et al.[31] for the polyimide, the alkyl segment is flanked on either side by large aminophenoxy groups, and the T_m of this segment itself is reduced by 81 °C as the alkyl spacer length increased from C_2 to C_{12} (Table 1 in ref 31). The T_g of the corresponding polymers is reduced by 95 °C (Table 4 of ref 31). In the work of Koning et al.,[32] the alkyl segment is placed between two large aromatic groups and the T_m was reduced by 262 °C. In the case of these polyimides, the high T_m is due to the aromatic groups, and an increase in the length of the alkyl spacer would reduce the aromatic interactions, resulting in lower T_m. The alkyl spacer itself might not become flexible. Similar reasoning could be applied to the case of *p*-phenylene-based liquid-crystalline polymers reviewed by Ober et al.[33] In the work of McKiernan et al.,[29b] the T_m of the α,ω-diols actually increased by 38 °C, as the length of the alkyl segment was increased from C_{13} to C_{44} (table 2 of ref 29b). This can be attributed to the OH group on either side of the alkyl segment, which is small compared with the large aromatic groups. The change in T_m is also small relative to the case of polyimides.

By comparing the melting temperatures in the present case (Figure 1 and Table S1 in the Supporting Information), we find that increasing the spacer length from C_6 to C_{12} does not lead to decrease in the T_m of the molecules as with the cases discussed above. Sandwiched between two hydrogen-bonding moieties, the longer alkyl spacer enhances the intermolecular van der Waals interaction and leads to higher melting temperatures. It is as if the hydrogen-bonding groups on the ends of the spacer act as anchors. Figure 1a shows that the melting temperatures (T_m) of these biscarbamates increase with the alkyl side chain length. The effect of the alkyl chain length on the T_m is more significant with the C_6 spacer than the C_{12}. With the shorter spacer, the T_m increases by 29 °C (from 91 to 120 °C) as the side-chain length increases from C_4 to C_{18}, whereas the increase is only 16 °C with the C_{12} spacer. In addition, with the $(CH_2)_6$ spacer, an increase of ~15 °C is seen between C_4 and C_8 side chains. However, the increase is only 7 °C with the C_{12} spacer. Thus, the effect of the alkyl side chain becomes less pronounced with the longer spacer. In both cases, the increase in T_m becomes less significant as the side-chain length increases (e.g., from C_{12} to C_{18}). Similar decrease in *increment* of T_m with an increase in side-chain length was also observed with aliphatic polyurethanes.[29] As mentioned above, with the C_4 side chain, the T_m is higher by 10 °C with the C_{12} spacer. With a short C_4 side chain, the van der Waals interaction promoted by the longer C_{12} spacer leads to an increase in T_m, relative to the C_6 spacer. The difference becomes less with an increase in side-chain length, and the T_m approaches that of short chain polyethylene with both spacers. Very little change in T_m is expected with longer alkyl side chains.

The van der Waals and hydrogen-bond interactions play a role in the variation of the T_m with the length of the spacer and the side chain. Let us consider the number of carbon atoms (including the carbonyl carbons) in the biscarbamate molecules with C_6 and C_{12} spacers. Figure 1b shows a plot of the T_m versus the number of carbon atoms in the biscarbamates. It is seen that irrespective of the spacer length, T_m values fall on the same curve. (We see the difference in the variation of T_m between the two cases in Figure 1a because the alkyl side chains are placed differently.) A common attribute is the contribution from the two hydrogen-bond moieties. The melting temperatures of *n*-alkanes are also plotted in Figure 1b. There is a difference of 71 °C in T_m between C_4–C_6 and hexadecane (both having 16 carbon atoms) due to the presence of two hydrogen bonds in the biscarbamate. We attribute the difference in the T_m of an *n*-alkane and the biscarbamate (having the corresponding number of alkyl carbon atoms) to the hydrogen-bond contribution. As the number of carbons in the molecule increases, the relative contribution of the hydrogen bonds decreases with respect to the van der Waals interaction. The difference in T_m is only 25 °C between C_{18}–C_{12} and pentacontane $[CH_3(CH_2)_{48}CH_3]$.

While the biscarbamates previously studied had hydrogen-bonding and van der Waals interactions, the purpose of introducing a phenyl termination (PhC_6–C_{12}) in this work was to include a third self-assembling code, namely, π–stacking. Such a system with three self-assembling codes is expected to be highly stabilized, with a high T_m. However, the phenyl-terminated PhC_6–C_{12} biscarbamate has a lower melting temperature (91.3 °C) than that of C_4–C_{12} biscarbamate (101.3 °C) (Figure 1). This could be due to the disruption in the conformational ordering of the alkyl side chains arising from the presence of bulky terminal phenyl groups and leads to the conclusion that the terminal phenyl groups act as defects. Figure 1c shows the variation of heat of fusion (ΔH) as a function of alkyl side-chain length. As with the T_m, the ΔH is larger for the biscarbamates with the C_{12} spacer and C_4 and C_8 side chains. With a side-chain length of C_{12} or longer, the difference in ΔH between the C_6 and C_{12} spacers becomes less significant. It is also seen that the heat of fusion of PhC_6–C_{12} biscarbamate is lower than that of the corresponding alkyl-terminated biscarbamate by a few tens of joules per gram of the sample, indicating less order. Thus, while multiple self-assembly codes can be viewed as an enabler in designing supramolecular systems, in our case, the presence of the phenyl end group does not add to the stability in terms of higher melting temperature or larger heat of fusion.

Morphology. Morphology of these biscarbamates was investigated with optical microscopy. Figure 2 shows the cross-polarized optical micrographs of the quenched (left) and SC (right) samples of the corresponding C_x–C_{12} biscarbamates. All of these samples exhibit spherulitic morphology, with the SC samples crystallizing with larger spherulites than the corresponding quenched samples. Of note is the observation that C_4–C_{12} (with the longer spacer) shows spherulitic morphology while C_4–C_6 did not.[8a]

Figure 3 shows the variation of the spherulite size with respect to the alkyl side-chain length and the type of terminal group for both quenched (Figure 3a) and SC (Figure 3b) samples. The spherulites of the SC samples are larger than those of quenched samples by a factor of more than an order of magnitude. The range of spherulite sizes is about the same with both C_6 and C_{12} spacers, varying from 80 to 200 μm for the quenched and from 500 to 2500 μm in the case of SC samples, depending on the length of the alkyl side chain.[8a] A maximum in spherulite size is seen for C_8–C_{12}, similar to the case of C_8–C_6. However, with a further increase in side-chain length, the spherulite size decreases for C_{12}–C_{12} and a sharp increase is seen for C_{18}–C_{12} for both quenched and SC samples. The

dx.doi.org/10.1021/jp309762a | J. Phys. Chem. B 2013, 117, 5705–5717

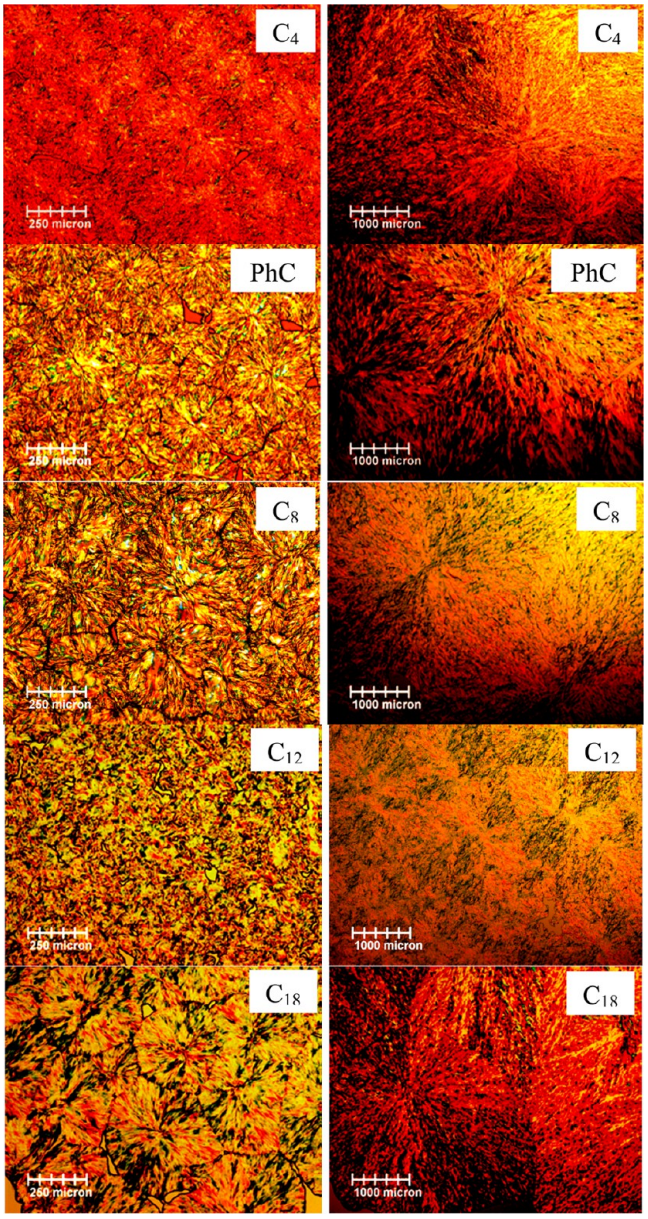

Figure 2. Optical micrographs of quenched (left) and slow-cooled (right) C_x–C_{12} biscarbamate samples with different alkyl side-chain length and terminal groups.

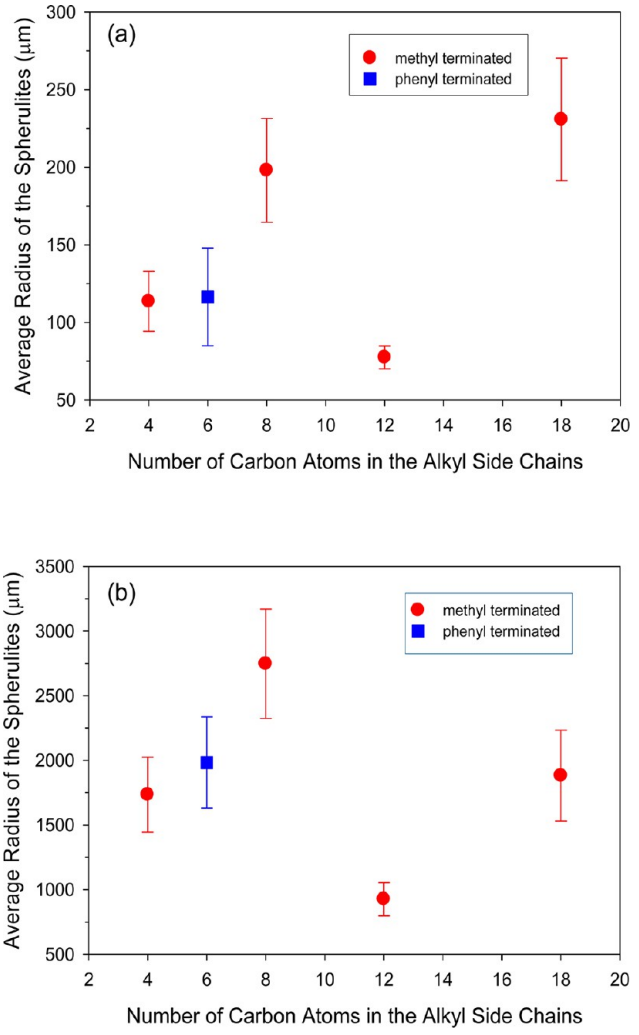

Figure 3. Variation of spherulite size of (a) quenched and (b) slow-cooled C_x–C_{12} biscarbamate samples as a function of alkyl side chain length and the type of terminal groups. (●) Methyl-terminated and (■) phenyl-terminated biscarbamates.

spherulitic growth is highly fibrous, consisting of twisted lamellae during isothermal growth. This is shown in Figure S2 in the Supporting Information for C_{12}–C_{12}. Figure 3 also shows that phenyl-terminated PhC_6–C_{12} biscarbamate forms smaller spherulites than the corresponding methyl-terminated biscarbamate.

Spherulite Growth Rate. The influence of alkyl side chain and spacer group length on crystallization of these molecules was further investigated with isothermal spherulite growth using hot-stage microscopy as described in the Experimental Section. For example, Figure S2 in the Supporting Information shows the micrographs of C_{12}–C_{12} recorded at different times of spherulite formation. It is seen that the spherulite grows radially with an extensive sequential branching of the lamellae. The size of the spherulites with time is shown in Figure 4a for the biscarbamates studied in this work. Because of the fast growth in the beginning, these plots do not extrapolate to a spherulite size of zero at t = 0 s. It is seen that the spherulite growth is complete due to impinging of the adjacent spherulites within 8 s for C_4–C_{12} and C_8–C_{12}, while it takes about 16 and 12 s for C_{12}–C_{12} and C_{18}–C_{12}, respectively. Such completion of growth occurs sooner with the C_{12} spacer. It was seen in our previous study that with C_6 spacers it took 20s for the C_{12}–C_6 and 28 s with C_{16}–C_6 and C_{18}–C_6 to complete the growth.[8a] Figure 4b shows the spherulite growth rate as a function of alkyl side-chain length. The spherulite growth rate increases from C_4–C_{12} to C_8–C_{12} with a minimum with C_{12}–C_{12}. Consistent with the time to complete the growth, the rate of growth is also higher with the C_{12} spacer. For example, with the C_8–C_{12}, the rate of spherulite growth is 160 μm/sec with the C_{12} spacer (Figure 4b), and it was 115 μm/sec with the C_8–C_6.[8a] The spherulite growth rate decreases significantly when the terminal methyl groups are replaced with phenyl groups.

Rate of Crystallization. While the spherulite growth data discussed above were obtained from optical microscopy, isothermal crystallization studies were performed with the DSC. The crystallization rates vary with the alkyl side-chain and spacer group lengths. Figure 5a shows the fractional heat of fusion (α) as a function of time for C_8–C_{12}, C_{12}–C_{12}, and C_{18}–

dx.doi.org/10.1021/jp309762a | J. Phys. Chem. B 2013, 117, 5705–5717

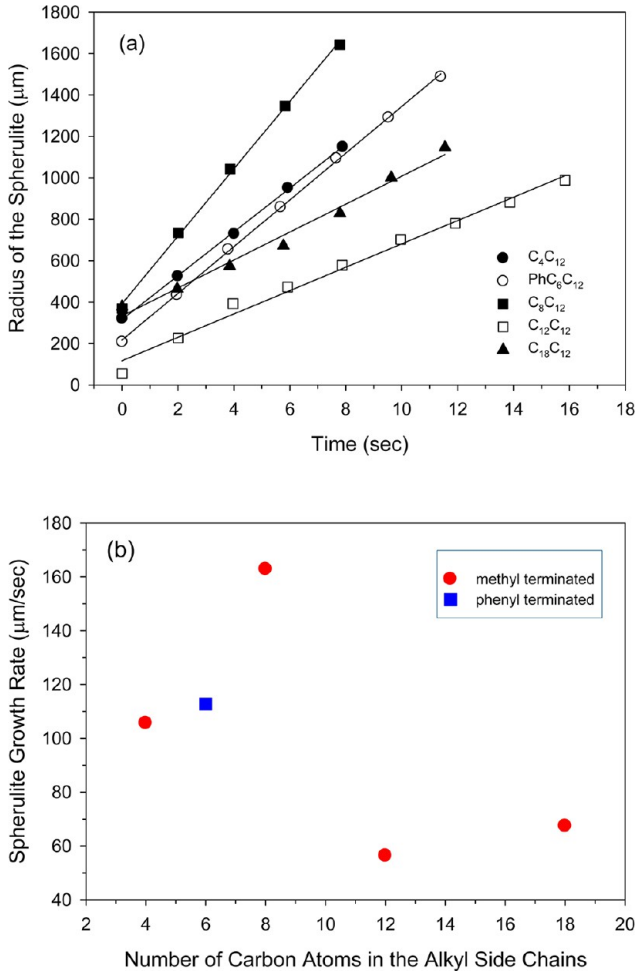

Figure 4. (a) Growth of spherulites with time and (b) rate of spherulite growth as a function of number of carbon atoms in the alkyl side chains of the biscarbamates.

C_{12} biscarbamates isothermally crystallized in the DSC. As noted with the variations in spherulite size and spherulite growth rate, a slower crystallization rate is seen for $C_{12}-C_{12}$ than the other two mentioned above. The $t_{1/2}$ (time required for 50% crystallization) values are 1.07, 1.70, and 1.09 min for C_8-C_{12}, $C_{12}-C_{12}$, and $C_{18}-C_{12}$, respectively. The differences in these values indicate that $C_{12}-C_{12}$ takes about twice the time to crystallize than the other two. Comparison of the rates of crystallization of C_x-C_{12} with those of previously studied C_x-C_6 biscarbamates[8a] shows that an increase in the spacer length significantly decreases the crystallization rate of these molecules. The $t_{1/2}$ values were 0.13 and 0.66 min, respectively, for C_8-C_6 and $C_{12}-C_6$.

Figure 5b shows a plot of the crystallization in terms of the Avrami equation for C_8-C_{12}, $C_{12}-C_{12}$, and $C_{18}-C_{12}$. It is seen from Table 1 that the value of n varies from 2.5 to 2.8 in the case of C_4-C_{12}, PhC_6-C_{12}, and $C_{18}-C_{12}$. Such values close to three indicate 3D growth of the nuclei and the nonintegral values denote constant radial growth of the spherulites. It is seen from Figure 5b that the plots for C_8-C_{12} and $C_{12}-C_{12}$ consist of two regions. There is a significant change in the slope after 20 ($\ln t = 2.98$) and 14.4 s ($\ln t = 2.67$), respectively. The change in slope occurs when the spherulite growth stops due to impingement and secondary crystallization stage begins. During the primary stage, the value of n is 3.1and 3.2 for C_8-C_{12} and

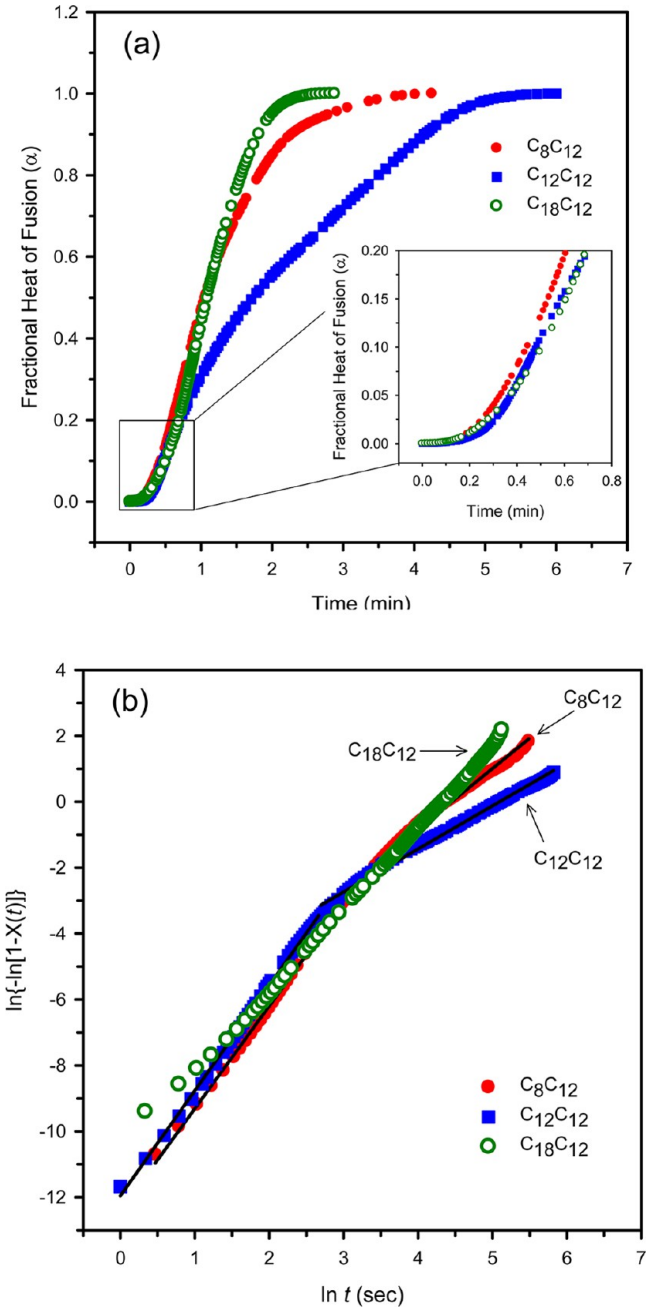

Figure 5. (a) Fractional heat of fusion of the biscarbamates as a function of time. (b) Plot in terms of the Avrami equation.

$C_{12}-C_{12}$, respectively. In the case of isothermal crystallization of poly(arylene ether ether ketone) (PEEK), similar two-stage crystallization was observed,[35a] and the primary stage, with n = 3, was associated with 3D growth and spherulite formation, with lamellae radiating from a central nucleus. The secondary stage in PEEK, with $n \approx 0.5$ was attributed to the formation of new crystals within the existing spherulites and lamellar thickening. In another study, Hsiao et al.[35b] found n = 4 for the primary crystallization with 3D growth during the isothermal crystallization of poly(ether ketone ketone) (PEKK) and n = 2 for the secondary crystallization. In the present case, we find that n reduces to 1.8 and 1.3, respectively, for C_8-C_{12} and $C_{12}-C_{12}$ during the second stage, which is diffusion-controlled.

dx.doi.org/10.1021/jp309762a | J. Phys. Chem. B 2013, 117, 5705−5717

Table 1. Avrami Parameters Calculated from Isothermal Crystallization Data

sample	Avrami exponent, n	K	$t_{1/2}$ (sec)
C_4C_{12}	2.79	2.14×10^{-6}	94
PhC_6C_{12}	2.46	3.12×10^{-5}	58
C_8C_{12}[a]	3.11	4.02×10^{-6}	48
C_8C_{12}[b]	1.84	2.79×10^{-4}	70
$C_{12}C_{12}$[c]	3.19	6.42×10^{-6}	38
$C_{12}C_{12}$[d]	1.31	1.28×10^{-3}	123
$C_{18}C_{12}$	2.46	2.29×10^{-5}	66

[a]Based on the first crystallization regime (data range: ln $t \leq 2.98$ (t = 19.8 s)). [b]Second crystallization regime (data range: ln $t \geq 2.98$). [c]First crystallization regime (data range: ln $t \leq 2.67$ (t = 14.4 s)). [d]Second crystallization regime (data range: ln $t \geq 2.67$ onward).

As noted above, the spherulite growth is complete in 8−16 s due to impingement, but the $t_{1/2}$ for crystallization is 1 to 2 min. Thus, crystallization continues after the growth of the spherulites. With the extensive branching of the fibrils during the growth of the spherulites (as in Figure S2 in the Supporting Information), the second stage of crystallization occurs due to the growth in the interfibrillar region and lamellar thickening.[35a] We might add that two-stage crystallization has not been reported as a routine occurrence in the literature. A search of SciFinder database for "two-stage crystallization" yielded about 10 cases of polymers and polymer blends, of which some of them were nonisothermal growth studies, and none on organic small molecules.

X-ray Diffraction. The X-ray diffraction profiles of the as-synthesized methyl-terminated biscarbamates with the C_{12} spacer showed an intense reflection with a large d spacing, and all of the others corresponding to smaller d spacings were weak. The reduction in the intensity of the wider angle reflections becomes more significant as the alkyl side-chain length increases, as seen from Figure S3 in the Supporting Information. This is found to be the case for both C_6 and C_{12} spacers.[8a,9] Figure 6a compares the X-ray diffraction traces for C_{18}−C_6 and C_{18}−C_{12}. In both cases, only a single reflection is of significant intensity, and the others are weak. Figure 6b shows, as an illustration, a plot of the ratio $I_{3.5}/I_{100}$ for the biscarbamates with C_{12} spacer and different alkyl chain lengths. Here $I_{3.5}$ is the intensity of the reflection with d = 3.5 Å, and I_{100} is the most intense reflection in each case. The 3.5 Å reflection was assigned to the distance between the hydrogen-bonding planes in our previous work with the C_6 spacers.[8a,9] It is seen that the intensity ratio becomes small with an increase in the alkyl side-chain length. This shows that even with the as-synthesized sample there is a preferential stacking of the molecule in one direction and that it becomes more significant as the length of the alkyl side chain increases.

Infrared Spectroscopy. Infrared spectroscopy of these molecules does not show any significant difference in the spectral profile of the SC and quenched samples, and the data presented here are of the former. Biscarbamates of this series show H-bonded N−H and C═O bands at around 3331 and 1682 cm^{-1}, respectively. The other two strong absorption bands corresponding to the symmetric and asymmetric stretching vibrations of CH_2 groups were observed at ∼2850 and ∼2920 cm^{-1}, respectively. A weak band at ∼2958 cm^{-1} and a very weak band at ∼2874 cm^{-1} corresponding to the C−H asymmetric and symmetric vibrations of the terminal CH_3 groups are also observed. These weak bands diminish with the

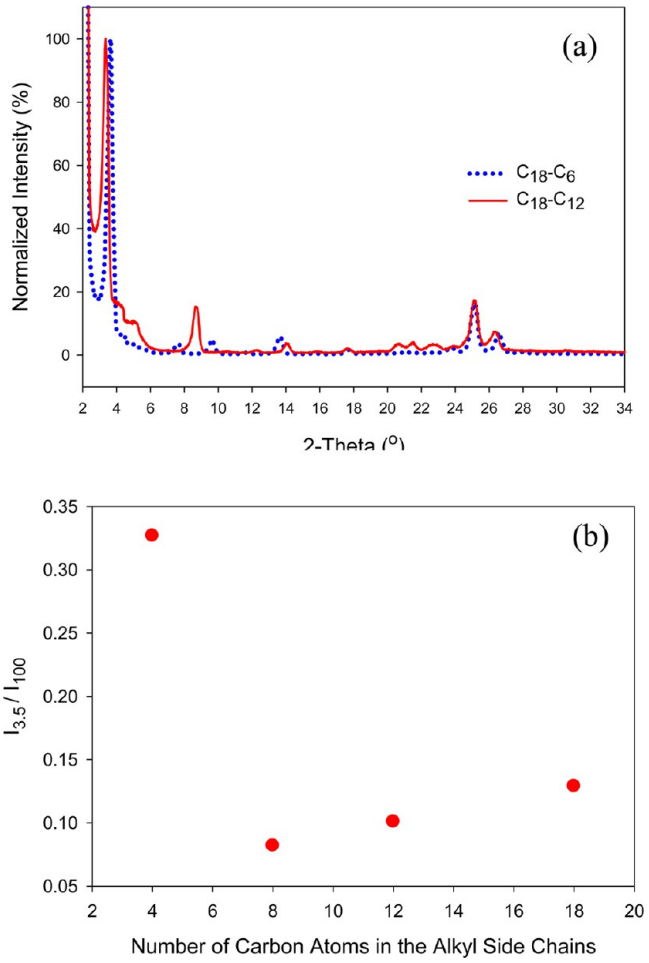

Figure 6. (a) XRD traces normalized to the highest intensity peak of C_{18}−C_6 and C_{18}−C_{12} biscarbamates and (b) the ratio of the peak intensity at d = 3.5 Å to that of the peak with highest intensity as a function of alkyl side chain length of C_x−C_{12} biscarbamates.

increased contribution of the CH_2 groups as the alkyl side chain length increases and vanish when the terminal CH_3 groups are replaced by phenyl groups, as shown in Figure 7a. Because of the difference in their bond order, the N−H group was found to be more susceptible to change in intermolecular interactions than the C═O group. A similar trend was seen with the symmetric and asymmetric CH_2 vibrations, where asymmetric vibrations were found to be more susceptible than the symmetric ones probably due to the energy differences related to these modes of vibrations. This trend is found to be common among the molecules within both the C_x−C_6 and C_x−C_{12} series and between the corresponding molecules of these two series. The N−H band of C_4−C_6 appears at 3324 cm^{-1} and shifts to 3319 cm^{-1} for C_{18}−C_6, while that of C_4−C_{12} appears at 3331 cm^{-1} and shifts to 3328 cm^{-1} for C_{18}−C_{12} (Figure 7b). However, the C═O bands appear at 1682 cm^{-1} for all of these molecules. The bands corresponding to ν_{as} and ν_s show a similar trend. The ν_{as} of C_4−C_6 appears at 2935 cm^{-1} and shifts to 2915 cm^{-1} for C_{18}−C_6, while ν_{as} of C_4−C_{12} appears at 2923 cm^{-1} and shifts to 2915 cm^{-1} for C_{18}−C_{12}. The difference in ν_{as} between C_4 and C_{18} molecules of both the series is more than that in ν_s.

There have been studies aimed at establishing a relationship between IR frequency shifts and hydrogen-bond distances in crystals.[36] Pimentel and Sederholm[36b] arrived at a simple

dx.doi.org/10.1021/jp309762a | J. Phys. Chem. B 2013, 117, 5705−5717

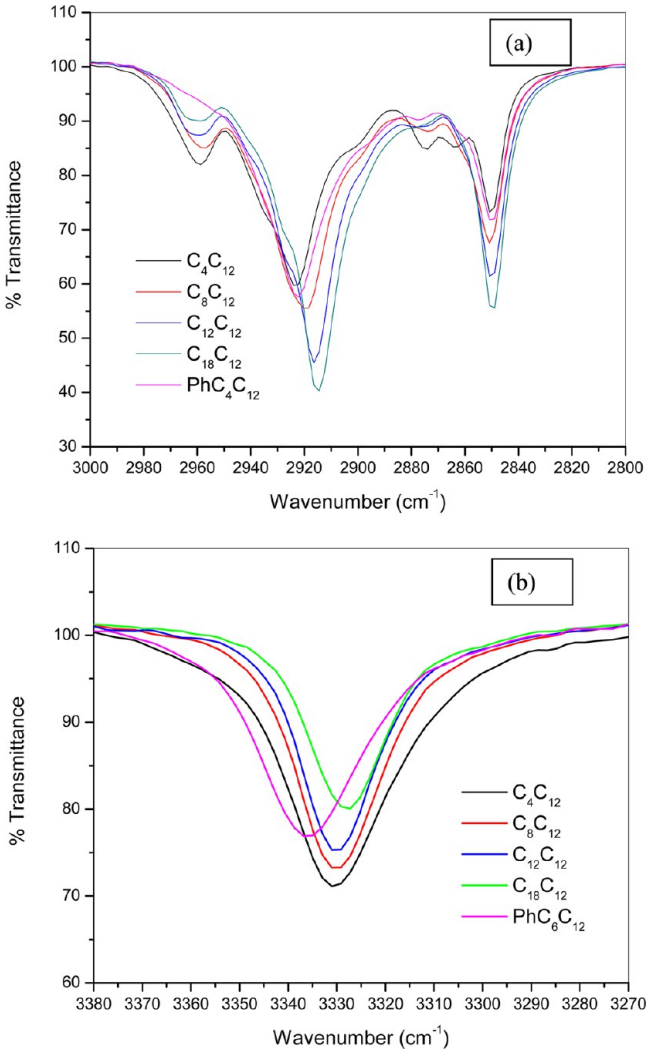

Figure 7. FTIR spectra of biscarbamates in the (a) CH_2 stretching and (b) N−H stretching regions.

relationship shown in eq 3 for the shift in the IR frequency of the N−H group in the N−H···O hydrogen bond:

$$\Delta\nu(\mathrm{cm}^{-1}) = 548(3.21 - R) \quad (3)$$

where R is the internuclear distance between the atoms N and O.

Bellamy and Owen[36d] developed a Lennard-Jones type of equation (eq 4):

$$\Delta\nu(\mathrm{cm}^{-1}) = 50[(d/R)^{12} - (d/R)^{6}] \quad (4)$$

where d = 3.4 for the N−H···O hydrogen bond and R is the internuclear distance between the atoms N and O. The peak position observed before[8a] for the N−H group in the C_x−C_6 series was 3320 cm^{-1}. Using a frequency of 3440 cm^{-1} for the non-hydrogen-bonded N−H group,[37] as observed in the cases of polyurethanes and polyamides, $\Delta\nu$ (cm^{-1}) = 120, leads to an N···O distance of 2.991 Å with eq 3 and 2.998 Å using eq 4. The N···O hydrogen-bond distance in the crystal structure[38] of C_{10}−C_6 was found to be 2.927 Å. The shorter distance could be attributed to the single-crystalline form. It is seen from Table 2 that the absorption frequency for the N−H group in C_x−C_{12} biscarbamates is ∼3330 cm^{-1}. With a $\Delta\nu$ of 110 cm^{-1} in this case, the N···O hydrogen-bond distance is 3.009 Å with eq 3 and 3.013 Å using eq 4. Thus, there is only an insignificant increase in the hydrogen-bond distance with the C_{12} spacer.

Table 2 shows that among the molecules of C_x−C_{12} series, the position of H-bonded N−H remains almost the same from C_4−C_{12} to C_{12}−C_{12} and shifts slightly to a lower wavenumber for C_{18}−C_{12}. The intensity of the peak decreases from C_4 to C_{12}, but the half width also decreases from 30.8 to 22.5 wave numbers. Figure 7 and Table 3 show that the ν_{as} changes significantly from C_4−C_{12} to C_{12}−C_{12}, indicating enhancement in van der Waals force with increased alkyl side-chain length. The intensity of the N−H band decreases while that of ν_{as} increases consistently with the increase in the alkyl side-chain length, indicating the relative decrease in the contribution of H-bond compared with van der Waals forces in molecular association. Thus it is likely that there is a balance between these two forces in the C_{12}−C_{12} molecule that contributes almost equally to all three directions of crystal growth. It should be noted that these molecules assemble through both H-bond and van der Waals forces in the H-bonding directions and with the aid of only van der Waals force in the other two directions. When the terminal groups of one of these molecules are replaced with phenyl groups, the H-bonded N−H and asymmetric C−H vibration bands appear at 3336 and 2923 cm^{-1}, respectively. The absorption frequencies of these two bands of PhC_6−C_{12} are higher than that of the corresponding

Table 3. Infrared Data for Symmetric (υ_s) and Asymmetric (υ_{as}) C−H Stretching Bands of Biscarbamates with Different Alkyl Side Chains

	asymmetric C−H		symmetric C−H	
sample ID	frequency (cm^{-1})	intensity	frequency (cm^{-1})	intensity
PhC_6−C_{12}	2923	42.5	2850	28.6
C_4−C_{12}	2923	40.5	2850	27.0
C_8−C_{12}	2919	44.6	2851	32.5
C_{12}−C_{12}	2916	54.5	2850	39.0
C_{18}−C_{12}	2915	60.0	2850	45.2

Table 2. Infrared Data for H-Bonded N−H and C═O Stretching Bands of Biscarbamates with Different Alkyl Side Chains

	H-bonded N−H			H-bonded C═O		
sample ID	frequency (cm^{-1})	intensity	fwhm (cm^{-1})[a]	frequency (cm^{-1})	intensity	fwhm (cm^{-1})
PhC_6−C_{12}	3336	23.2	27.1	1683	61.9	20.5
C_4−C_{12}	3331	28.9	30.8	1682	65.1	22.1
C_8−C_{12}	3330	26.9	22.9	1683	60.0	20.8
C_{12}−C_{12}	3330	24.9	23.0	1684	57.2	18.7
C_{18}−C_{12}	3328	20.0	22.5	1684	53.8	18.7

[a]Full width at half-maximum.

dx.doi.org/10.1021/jp309762a | J. Phys. Chem. B 2013, 117, 5705−5717

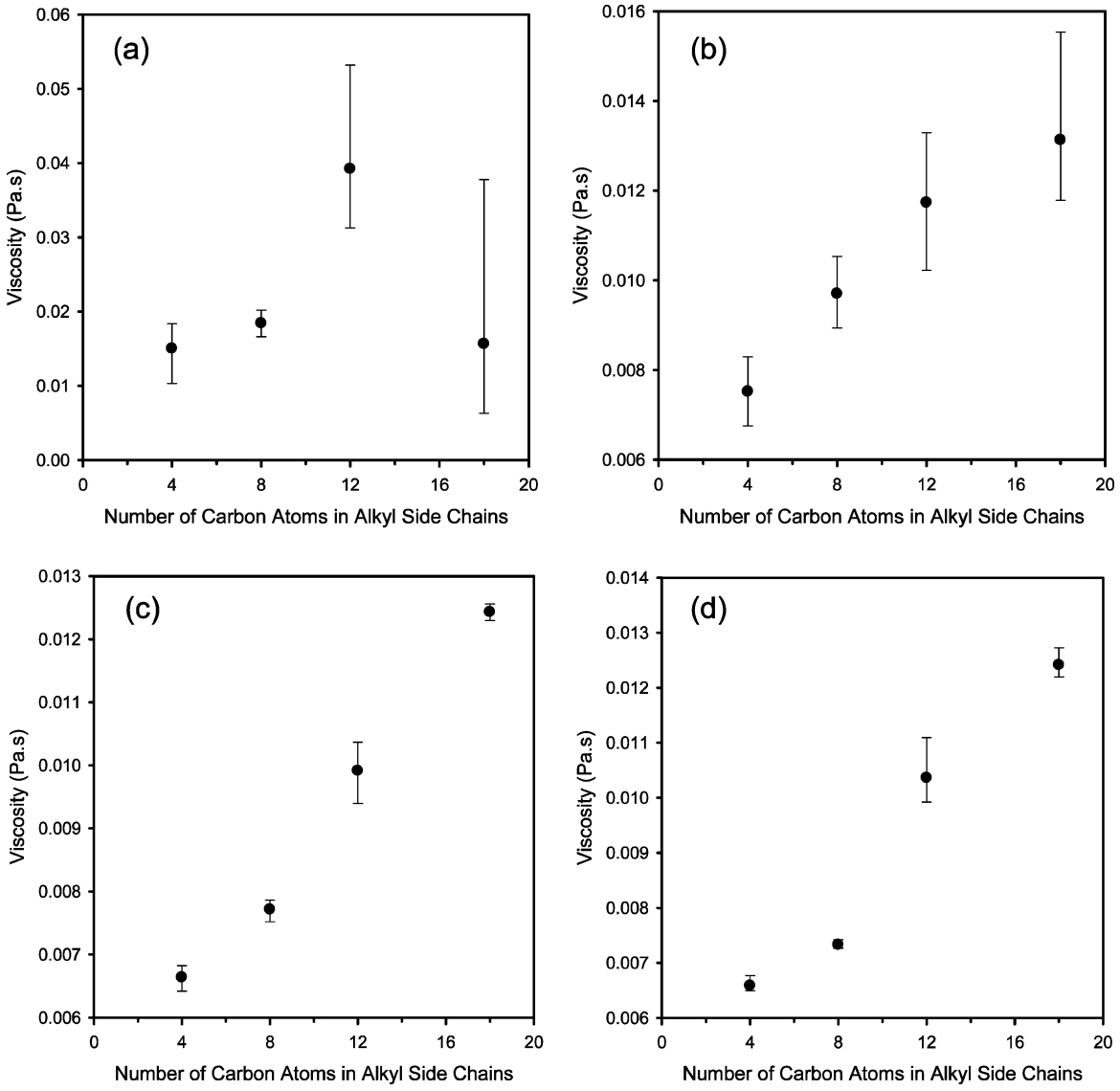

Figure 8. Variation in the melt viscosity of the C_x−C_{12} biscarbamates as a function of the number of carbon atoms in the alkyl side chains. Viscosity measured at different shear rates: (a) 1, (b) 10, (c) 50, and (d) 100 s^{-1}.

methyl-terminated molecule. The shifts of these bands to higher wave numbers compared with the corresponding methyl-terminated molecule indicate that both the H-bond and van der Waals forces are less strong in this molecule. The bulky phenyl groups seem to prevent closer packing of these molecules due to conformational mismatch instead of enhancing it through π−π interactions. These observations are consistent with the lower melting temperature and smaller heat of fusion of the PhC_6−C_{12} molecule compared with the methyl-terminated molecules, which has an even smaller number of carbon atoms in the alkyl side chain.

Melt Viscosity. It was mentioned in the Introduction that the low melt viscosity of (8−12 cP or 0.008 to 0.012 Pa·s) of carbamates with alkyl side chains makes them candidates for ink vehicles in inkjet printing technology.[25−27] Here we examined the influence of the length of the alkyl side chain on the melt viscosity. Shear rates from 0.1 to100 s^{-1} were used. Figure 8 shows the variation of viscosity with alkyl chain length for four shear rates. At a very low shear rate, the experimental error is large. However, a uniform trend of increase in η with alkyl chain length is seen with higher shear rates. For example, with 10 s^{-1}, η = 0.0075 Pa·s for C_4−C_{12} and it increases to 0.013 for C_{18}−C_{12}. Considering that propulsion of the ink in an inkjet printer would involve shear, these values are in the range specified for their application.[27] We further note that the samples are shear-thinning. For C_4−C_{12}, η = 0.0575 Pa·s with a shear rate of 0.1 s^{-1}, and it decreases to 0.0066 Pa·s with 100 s^{-1}. Even with a longer side chain, for C_{18}−C_{12} the value of η decreases from 0.1744 Pa·s at 0.1 s^{-1} to 0.0124 with a shear rate of 100 s^{-1}. The decrease in η with shear rate is shown in Figure 9. The alignment and orientation of these hydrogen-bondable molecules caused by shear give rise to the observed shear-thinning behavior. We have shown before[8b] that organogels of these types of biscarbamates could be prepared with oriented fiber morphology by simply stirring the solution with a magnetic stirrer during gelation. Shear thinning behavior (as commonly seen with honey) has been reported in hydrogen-bonded systems such as certain polysaccharides,[39] poly(vinyl alcohol),[40] as well as liquid-crystalline polymers.[41] The carbamates are model compounds for polyurethanes. The shear thinning behavior of polyurethanes (e.g., in aqueous media) has been described in patent literature.[42] There has

dx.doi.org/10.1021/jp309762a | J. Phys. Chem. B 2013, 117, 5705−5717

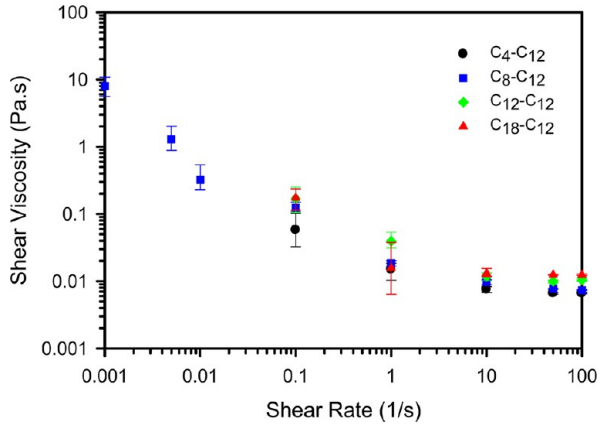

Figure 9. Variation of shear viscosity with shear rate for C_4–C_{12}, C_8–C_{12}, C_{12}–C_{12}, and C_{18}–C_{12}.

been no previous report of shear-thinning of carbamates, biscarbamates, or ureas in the melt.

CONCLUSIONS

We studied the thermal properties and morphology of a series of homologous biscarbamate molecules with a longer spacer group than those in our previous work. Whereas it might be expected that a longer spacer would lead to more conformational flexibility, we find that it is not the case with these molecules. A number of studies in the literature found a decrease in transition temperatures with an increase in spacer length, and this behavior was attributed to increased flexibility afforded by the longer spacers. We believe that such behavior is due not to an increase in the flexibility of the alkyl spacer but to the disruption of, for example, aromatic interactions with the longer spacer. With the biscarbamates discussed here, the presence of the hydrogen-bonding group on either end of the spacer acts as a "peg" to make the C12 segment less flexible. With both C_6 and C_{12} spacers, we find that the maximum in the spherulite size as well as the rate of spherulite growth occur with an alkyl side chain length of C_8. The Avrami analysis of crystallization shows that C_8–C_{12} and C_{12}–C_{12} follow two-stage crystallization. Along this series of molecules, a minimum spherulite size, spherulite growth rate, and rate of crystallization were observed for this symmetric C_{12}–C_{12} biscarbamate. The two-stage crystallization observed here can be attributed to the fast self-assembly of the molecules driven by the hydrogen bond and van der Waals interactions and subsequent perfection of the crystalline order. As discussed above, two-stage crystallization has been known for a few polymer systems but not for organic small molecules. The hydrogen bonding and van der Waals interactions along the sheets of these molecules cause shear thinning. Such shear thinning has been reported for polyurethanes in the patent literature, but we are not aware of such reports on ureas or carbamates. The phenyl terminal groups do not add another self-assembly code, that is, π-interaction, but act as defects. With a bulky phenyl terminal group, the melting temperature, heat of fusion, and the spherulite size of the molecule decreased significantly. These structural features thus provide extra knobs to tune the functional properties of these molecules.

ASSOCIATED CONTENT

Supporting Information

DSC curves of C_{12}–C_{12} and PhC_6–C_{12}; optical micrographs of spherulite growth of C_{12}–C_{12} with time, X-ray diffraction, and a table of melting temperatures. This material is available free of charge via the Internet at http://pubs.acs.org.

AUTHOR INFORMATION

Corresponding Author

*E-mail: Sundar@Carleton.ca.

Notes

The authors declare no competing financial interest.

ACKNOWLEDGMENTS

Financial support from the Natural Sciences and Engineering Research Council of Canada (NSERC) is gratefully acknowledged. We thank Professor Savvas G. Hatzikiriakos and Dr. Mahmoud Ansari, Department of Chemical and Biological Engineering, The University of British Columbia for the melt viscosity measurements.

REFERENCES

(1) (a) *Supramolecular Assembly via Hydrogen Bonds II*; Mingos, D. M. P. Ed.; Springer: New York, 2004. (b) Lehn, J.-M. *Supramolecular Chemistry*; VCH: Weinheim, Germany, 1995. (c) Ikeda, M.; Nobori, T.; Schmutz, M.; Lehn, J.-M. Hierarchical Self-Assembly of a Bow-Shaped Molecule Bearing Self-Complementary Hydrogen Bonding Sites into Extended Supramolecular Assemblies. *Chem.—Eur. J.* **2005**, *11*, 662–668.

(2) Zimmerman, S. C.; Corbin, P. S. Heteroaromatic Modules for Self-Assembly Using Multiple Hydrogen Bonds. *Struct. Bonding (Berlin)* **2000**, *94*, 63–94.

(3) (a) Tew, G. N.; Scott, R. W.; Klein, M. L.; Degrado, W. F. De Novo Design of Antimicrobial Polymers, Foldamers, and Small Molecules: From Discovery to Practical Applications. *Acc. Chem. Res.* **2010**, *43*, 30–39. (b) Hill, D. J.; Mio, M. J.; Prince, R. B.; Hughes, T. S.; Moore, J. S. A Field Guide to Foldamers. *Chem. Rev.* **2001**, *101*, 3893–4011. (c) Horne, W. S.; Gellman, S. H. Foldamers with Heterogeneous Backbones. *Acc. Chem. Res.* **2008**, *41*, 1399–1408. (d) Gellman, S. H. Foldamers: A Manifesto. *Acc. Chem. Res.* **1998**, *31*, 173–180.

(4) (a) Yang, X.; Martinovic, S.; Smith, R. D.; Gong, B. Duplex Foldamers from Assembly Induced Folding. *J. Am. Chem. Soc.* **2003**, *125*, 9932–9933. (b) Sanford, A. R.; Yamato, K.; Yang, X.; Yuan, L.; Han, Y.; Gong, B. Well-Defined Secondary Structures: Information-Storing Molecular Duplexes and Helical Foldamers Based on Unnatural Peptide Backbones. *Eur. J. Biochem.* **2004**, *271*, 1416–1425. (c) Archer, E. A.; Gong, H.; Krische, M. J. Hydrogen Bonding in Noncovalent Synthesis: Selectivity and the Directed Organization of Molecular Strands. *Tetrahedron* **2001**, *57*, 1139–1159.

(5) (a) Astruc, D.; Boisselier, E.; Ornelas, C. Dendrimers Designed for Functions: From Physical, Photophysical, and Supramolecular Properties to Applications in Sensing, Catalysis, Molecular Electronics, Photonics, and Nanomedicine. *Chem. Rev.* **2010**, *110*, 1857–1959. (b) Rosen, B. M.; Wilson, C. J.; Wilson, D. A.; Peterca, M.; Imam, M. R.; Percec, V. Dendron-Mediated Self-Assembly, Disassembly, and Self-Organization of Complex Systems. *Chem. Rev.* **2009**, *109*, 6275–6540. (c) Huang, B.; Parquette, J. R. Effect of an Internal Anthranilamide Turn Unit on the Structure and Conformational Stability of Helically Biased Intramolecularly Hydrogen-Bonded Dendrons. *J. Am. Chem. Soc.* **2001**, *123*, 2689–2690.

(6) Brunsveld, L.; Folmer, B. J. B.; Meijer, E. W.; Sijbesma, R. P. Supramolecular Polymers. *Chem. Rev.* **2001**, *101*, 4071–4097.

(7) (a) Moniruzzaman, M.; Goodbrand, B.; Sundararajan, P. R. Morphology and Thermal Behavior of Self-Assembling Carbamates. *J. Phys. Chem. B* **2003**, *107*, 8416–8423. (b) Moniruzzaman, M.;

Sundararajan, P. R. Low Molecular Weight Organogels Based on Long-Chain Carbamates. *Langmuir* **2005**, *21*, 3802−3807.
(8) (a) Khanna, S.; Moniruzzaman, M.; Sundararajan, P. R. Influence of Single versus Double Hydrogen-Bonding Motif on the Crystallization and Morphology of Self-Assembling Carbamates with Alkyl Side Chains: Model System for Polyurethanes. *J. Phys. Chem. B* **2006**, *110*, 15251−15260. (b) Khanna, S.; Khan, M. K.; Sundararajan, P. Influence of Double Hydrogen Bonds and Alkyl Chains on the Gelation of Nonchiral Polyurethane Model Compounds: Sheets, Eaves Trough, Tubes and Oriented Fibers. *Langmuir* **2009**, *25*, 13183−13193.
(9) Khan, M. K.; Sundararajan, P. R. Effects of Carbon Atom Parity and Alkyl Side Chain Length on the Crystallization and Morphology of Biscarbamates, A Set of Model Compounds for Polyurethanes. *J. Phys. Chem. B* **2011**, *115*, 8696−8706.
(10) Gaylord, N. G. Carbamates. III. Reactions of "Acetylene Bis-Carbamates". *J. Org. Chem.* **1955**, *20*, 546−548.
(11) (a) Furer, V. L. Hydrogen Bonding in Ethyl Carbamate Studied by IR Spectroscopy. *J. Mol. Struct.* **1998**, *449*, 53−59. (c) Furer, V. L. The IR Spectra, Hydrogen Bonding and Conformations of Aliphatic and Aromatic Epoxy Carbamates. *J. Mol. Struct.* **1999**, *513*, 1−8. (b) Furer, V. L. The IR Spectra and Hydrogen Bonding of Toluene-2,6-Bis(methyl) and 4,4′-Diphenylmethane-bis(methyl) Carbamates. *J. Mol. Struct.* **2000**, *520*, 117−123.
(12) Martinek, T. W.; Klass, D. L. Glycol bis-Carbamates. U.S. Patent, 3,335,139, 1967.
(13) Atwell, G. J.; Fan, J.-Y.; Tan, K.; Denny, W. A. DNA-Directed Alkylating Agents. 7. Synthesis, DNA Interaction, and Antitumor Activity of Bis(hydroxymethyl)- and Bis(carbamate)-Substituted Pyrrolizines and Imidazoles. *J. Med. Chem.* **1998**, *41*, 4744−4754.
(14) Papot, S.; Bachmann, C.; Combaud, D.; Gesson, J.-P. Study of Biscarbamates Derived from 2-Aminobenzylamines as Models for Alcohol Prodrugs. *Tetrahedron* **1999**, *55*, 4699−4708.
(15) Chueca, A.; Baron, M.; Lopez, G. J. Are Bis-carbamates Photosynthetic Inhibitors by Root Application? *Photosynth., Proc. Int. Congr., 5th* **1981**, *6*, 555−563. *Chem. Abstr.* **1981**, *97*, 50917.
(16) Anderson, W. K.; Mach, R. H. Synthesis, Chemical Reactivity, and Antileukemic Activity of 5-Substituted 6,7-Bis(hydroxymethyl)-pyrrolo[1,2-c]thiazole Biscarbamates and the Corresponding Sulfoxides and Sulfones. *J. Med. Chem.* **1987**, *30*, 2109−2115.
(17) Chambers, J.; Reese, C. B. The Thermal Decomposition of Some Tolylene Bis Carbamates. *Br. Polym. J.* **1977**, *9*, 41−46.
(18) Matzger, A. J.; Kim, K. Ordering of Oligourethanes on Surfaces. *PMSE Prepr.* **2003**, *89*, 825−826.
(19) Steichele, K. Polyurethane Composition. Belgian Patent BE 882,922, 1980
(20) Saka, K.; Noda, K. Urethane and/or Urea Waxy Compositions with Good Hardness for Adhesives, Sealants, and Binders, *Jpn. Kokai Tokkyo Koho* 1987, JP 62 179 584; *Chem. Abstr.* **1987**, *108*, 39820r.
(21) Tanaka, K.; Kano, Y.; Yoshida, K. Agents for Improving Low-temperature Fluidity of Fuel Oils. *Jpn. Kokai Tokkyo Koho* **1988**, JP 63248894; *Chem. Abstr.* **1988**, *110*, 79137w.
(22) Kinoshita, H.; Sekiya, M.; Mishima, M. Urea-Urethane Lubricating Grease Composition. Eur. Patent EP 274 756, 1988
(23) Rohr, W.; Franke, A.; Giertz, H.; Amann, A. Biscarbamates. British Patent GB 1396523, 1975.
(24) D'Silva, T. D. J. Pesticidal Symmetrical Bis(sulfenylated) Biscarbamate Compounds. U.S. Patent 4,400,389, 1983.
(25) Dai Nippon Printing Co., Ltd., Japan. Urethane Compound. *Jpn. Kokai Tokkyo Koho* **1983**, JP 58201758; *Chem. Abstr.* **1983**, *110*, 174289z.
(26) Tanaka, T.; Yoshitomi, T.; Hanada Y.; Ohashi, M.; Takeda, Y. Thermal-transfer Recording Material *Jpn. Kokai Tokkyo Koho* 1987, JP 62 090 289; *Chem Abstr.* **1987**, *107*, 208963.
(27) Goodbrand, B.; Boils, D.; Sundararajan, P. R.; Wong, R.; Malhotra, S. Ink Compositions Containing Thioureas or Oximes U.S. Patent 6,187,082, 2001.
(28) Khan, M. K.; Sundararajan, P. R. Molecular Selectivity and Immiscibility During the Crystallization of Mixtures of a Set of Homologous Self-Assembling Molecules. *J. Phys. Chem. B* **2008**, *112*, 4223−4232.
(29) (a) McKiernan, R. L.; Heintz, A. M.; Hsu, S. L.; Atkins, E. D. T.; Penelle, J.; Gido, S. P. Influence of Hydrogen Bonding on the Crystallization Behavior of Semicrystalline Polyurethanes. *Macromolecules* **2002**, *35*, 6970−6974. (b) McKiernan, R. L.; Gido, S. P.; Penelle, J. Synthesis and Characterization of Polyethylene-like Polyurethanes Derived from Long-chain, Aliphatic α-ω Diols. *Polymer* **2002**, *43*, 3007−3017. (c) McKierman, R. L.; Heintz, A. M.; Hsu, S. L.; Gido, S. P.; Penelle, J. From Aliphatic Polyurethanes to Linear Polyethylene: Influence of Hydrogen Bonding on the Morphology of Semi-Crystalline Polymers. *PMSE Prepr.* **2001**, *84*, 416−417.
(30) Ehrenstein, M.; Dellsperger, S.; Kocher, C.; Stutzmann, N.; Weder, C.; Smith, P.; New, P. Polyamides with Long Alkane Segments: Nylon 6.24 and 6.34. *Polymer* **2000**, *41*, 3531−3539.
(31) Yin, J.; Ye, Y.-F.; Wang, Z.-G. Study on Preparation and Properties of Polyimides Containing Long Flexible Chains in the Backbone. *Eur. Polym. J.* **1998**, *34*, 1839−1843.
(32) Koning, C.; Teuwen, L.; Meijer, E. W.; Moonen, J. Synthesis and Properties of α,ω-Diaminoalkane Based Polyimides. *Polymer* **1994**, *35*, 4889−4895.
(33) (a) Ober, C. K.; Jin, J. I.; Lenz, R. W. Liquid Crystal Polymers with Flexible Spacers in the Main Chain. *Adv. Polym. Sci.* **1984**, *59*, 103−146. (b) Ober, C. K.; Bluhm, T. L. *Current Topics in Polymer Science*; Ottenbrite, R. M., Utracki, L. A., Inoue, S., Eds.; Hanser Publishers: New York, 1987; Chapter 4.3, Vol. *1*, pp 249−290.
(34) Goodbrand, B.; Boils, D.; Sundararajan, P. R.; Wong, R. Acoustic Printing Inks Containing Bis(carbamates) in Vehicle. U.S. Patent, 6,414,051, 2002.
(35) (a) Marand, H.; Alizadeh, A.; Farmer, R.; Desai, R.; Vesselin, V. Influence of Structural and Topological Constraints on the Crystallization and Melting Behavior of Polymers. 2. Poly(arylene ether ether ketone). *Macromolecules* **2000**, *33*, 3392−3403. (b) Hsiao, B. S.; Chang, I. Y.; Sauer, B. B. Isothermal Crystallization Kinetics of Poly(ether ketone ketone) and Its Carbon-Fibre-Reinforced Composites. *Polymer* **1991**, *32*, 2799−2805.
(36) (a) Nakamoto, K.; Margoshes, M.; Rundle, R. E. Stretching Frequencies as a Function of Distances in Hydrogen Bonds. *J. Am. Chem. Soc.* **1955**, *77*, 6480−6486. (b) Pimentel, G. C.; Sederholm, C. H. Correlation of Infrared Stretching Frequencies and Hydrogen Bond Distances in Crystals. *J. Chem. Phys.* **1956**, *24*, 639−641. (c) Bellamy, L. J.; Pace, R. J. The Significance of Infra-red Frequency Shifts in Relation to Hydrogen Bond Strengths. *Spectrochim. Acta* **1969**, *25A*, 319−328. (d) Bellamy, L. J.; Owen, A. J. A Simple Relationship Between the Infra-red Stretching Frequencies and the Hydrogen Bond Distances in Crystals. *Spectrochim. Acta* **1969**, *25A*, 329−333.
(37) (a) Coleman, M. M.; Lee, K. H.; Skrovanek, D. J.; Painter, P. C. Hydrogen Bonding in Polymers. 4. Infrared Temperature Studies of a Simple Polyurethane. *Macromolecules* **1986**, *19*, 2149−2157. (b) Moriya, K.; Minagawa, T.; Yano, S. Infrared Spectroscopic Studies of Thermotropic Polyamides. *Polym. Bull.* **1994**, *33*, 209−213.
(38) Alimova, L. L.; Atovmyan, E. G.; Filipenko, O. S. The Crystal and Molecular Structure of Hexamethylene-1,6-(O,O′-didecyl)-diurethane. *Kristallografiya* **1987**, *32*, 97−101 (article in Russian).
(39) (a) Li, X.; Al-Assaf, S.; Fang, Y.; Phillips, G. O. Characterisation of Commercial LM-Pectin in Aqueous Solution. *Carbohydr. Polym.* **2013**, *92*, 1133−1142. (b) Zhang, Y.; Xu, X.; Zhang, L. Gel Formation and Low-Temperature Intramolecular Conformation Transition of a Triple-Helical Polysaccharide Lentinan in Water. *Biopolymers* **2008**, *89*, 852−861. (c) Tako, M. Molecular Origin for the Thermal Stability of Schizophyllan. *Polym. Gels Networks* **1996**, *4*, 303−313.
(40) (a) Gao, H.; He, J.; Yang, R.; Yang, L. Characteristic Rheological Features of High Concentration PVA Solutions in Water with Different Degrees of Polymerization. *J. Appl. Polym. Sci.* **2010**, *116*, 2734−2741. (b) Lyoo, W. S.; Kim, J. H.; Choi, J. H.; Kim, B. C.; Blackwell, J. Role of Degree of Saponification in the Shear-Induced Molecular Orientation of Syndiotacticity-Rich Ultrahigh Molecular Weight Poly(vinyl alcohol). *Macromolecules* **2001**, *34*, 3982−3987.

(41) Walker, L. M.; Kernick, W. A.; Wagner, N. J. *In Situ* Analysis of the Defect Texture in Liquid Crystal Polymer Solutions under Shear. *Macromolecules* **1997**, *30*, 508−514.
(42) Milbocker, M. T.; Wilson, J. A. Reversibly Gelling Polyurethane Composition for Surgical Repair and Augmentation. European Patent, WO 2007089484, 2007; U.S. Patent, U.S. 8,114,157, 2012.